communications
earth & environment

ARTICLE

https://doi.org/10.1038/s43247-021-00193-9 OPEN

Absolute seasonal temperature estimates from clumped isotopes in bivalve shells suggest warm and variable greenhouse climate

Niels J. de Winter [1,2]✉, Inigo A. Müller [1], Ilja J. Kocken [1], Nicolas Thibault [3], Clemens V. Ullmann[4], Alex Farnsworth [5,6], Daniel J. Lunt[5], Philippe Claeys [2] & Martin Ziegler [1]

Seasonal variability in sea surface temperatures plays a fundamental role in climate dynamics and species distribution. Seasonal bias can also severely compromise the accuracy of mean annual temperature reconstructions. It is therefore essential to better understand seasonal variability in climates of the past. Many reconstructions of climate in deep time neglect this issue and rely on controversial assumptions, such as estimates of sea water oxygen isotope composition. Here we present absolute seasonal temperature reconstructions based on clumped isotope measurements in bivalve shells which, critically, do not rely on these assumptions. We reconstruct highly precise monthly sea surface temperatures at around 50 °N latitude from individual oyster and rudist shells of the Campanian greenhouse period about 78 million years ago, when the seasonal range at 50 °N comprised 15 to 27 °C. In agreement with fully coupled climate model simulations, we find that greenhouse climates outside the tropics were warmer and more seasonal than previously thought. We conclude that seasonal bias and assumptions about seawater composition can distort temperature reconstructions and our understanding of past greenhouse climates.

[1] Department of Earth Sciences, Faculty of Geosciences, Utrecht University, Utrecht, the Netherlands. [2] AMGC research group, Vrije Universiteit Brussel, Brussels, Belgium. [3] Faculty of Science, IGN, University of Copenhagen, Copenhagen, Denmark. [4] Camborne School of Mines and Environment and Sustainability Institute, University of Exeter, Penryn, UK. [5] School of Geographical Sciences, University of Bristol, Bristol, UK. [6] State Key Laboratory of Tibetan Plateau Earth System Science (LATPES), Institute of Tibetan Plateau Research, Chinese Academy of Sciences, Beijing, Beijing, China. ✉email: n.j.dewinter@uu.nl

Seasonal extremes were of vital importance for the evolution and distribution of life over geological history[1]. The effects of greenhouse warming on seasonal variability in temperature and the hydrological cycle are still poorly constrained[2,3], while being of considerable interest for projecting future climate and its impact on the ongoing biodiversity crisis[4–6]. Reconstructions of deep time (pre-Quaternary) greenhouse periods yield valuable insights into the dynamics of warm climates and the ecological response to forcing mechanisms such as rising atmospheric CO_2 levels[7,8]. Accurate reconstructions are imperative to evaluate climate model predictions under dissimilar climate states[9,10]. Particularly seasonal range is poorly constrained with little quantitative evidence. The warm, ice free Late Cretaceous period presents a valuable reference period to assess seasonal variability under greenhouse conditions[11,12].

Reconstructions based on stable oxygen isotope ratios ($\delta^{18}O_c$) in marine carbonates and organic paleothermometry (e.g. TEX_{86}) indicate that Late Cretaceous global mean sea surface temperatures (SST) were ~5–6 °C warmer than today[11–13] with a reduced latitudinal temperature gradient (an "equable climate"[14]), while exhibiting limited temperature seasonality[15,16]. However, the reliability of many past seasonal reconstructions is undermined by seasonal bias and poorly constrained assumptions of seawater composition ($\delta^{18}O_{sw}$ bias[17]). This hampers our understanding of past warm climates and hinders accurate evaluation of climate models[16,18,19].

Seasonal bias occurs if a proxy is interpreted as representing annual mean conditions but is in fact biased to a particular season[17]. Since fossil species producing the material that constitutes SST archives may not have a close modern relative for proxy calibration[20], uncertainties about their growth seasons may unpredictably bias reconstructions[21]. Seawater oxygen isotope composition ($\delta^{18}O_{sw}$) is an important input parameter into the widely used carbonate $\delta^{18}O_c$ temperature proxy[22], but it is highly variable across ocean basins (−3‰ to +2‰VSMOW[23–25]) and remains poorly constrained across geological timescales[26,27]. Biases in assumed $\delta^{18}O_{sw}$ composition thus undermine SST reconstructions, especially those from highly variable epicontinental seas[28].

The advent of carbonate clumped isotope (Δ_{47}) SST reconstructions on a seasonal scale promises to eliminate these two biases[17,29]. The clumped isotope thermometer yields accurate SST reconstructions independent of $\delta^{18}O_{sw}$ assumptions[30]. It also allows the reconstruction of $\delta^{18}O_{sw}$, yielding information about the (local) hydrological cycle, an important aspect of climate rarely constrained in deep time, rectifying bias in the popular carbonate $\delta^{18}O_c$ temperature proxy. Recent advances in clumped isotope instrumentation and standardization have reconciled previous inter-lab disagreements and shown that many carbonate paleoarchives (e.g. foraminifera, bivalves, and eggshells) conform to the theoretical Δ_{47} temperature calibration with negligible influence of isotope disequilibrium[31,32] (see Supplementary Discussion). The large sample sizes required for individual Δ_{47}-based temperature estimates (>2 mg) have complicated paleoseasonality reconstructions using this accurate method[33], but a recently developed statistical approach enables its use for seasonality reconstructions[17].

Here we use clumped isotope analyses on microsampled (~100 μg) profiles through fossil bivalve shells to obtain, for the first time, absolute SST and $\delta^{18}O_{sw}$ seasonality reconstructions of a greenhouse climate. We apply this new method on well-preserved oyster (*Rastellum diluvianum* and *Acutostrea incurva*) and rudist (*Biradiolites suecicus*) shells from Campanian (78.1 ± 0.3 Ma[34]) coastal localities of the Kristianstad Basin in southern Sweden (46 ± 3°N paleolatitude[35]; see Fig. 1 and "Methods"). We compare these reconstructions with fully coupled climate model simulations of the Campanian greenhouse (see "Methods") to explore their implications for Late Cretaceous greenhouse climate.

Results

All specimens showed clear seasonal $\delta^{18}O_c$ fluctuations of −2.0–0.0‰ in *R. diluvianum*, −2.0–0.0‰ in *A. incurva* and −2.7‰ to −1.0‰ in *B. suecicus* on which shell chronologies were based (see "Methods"). The assumption that periodic $\delta^{18}O_c$ fluctuations reflect seasonality is demonstrated to be a valid basis for constructing intra-shell chronologies in nearly all modern environments[17]. Seasonal $\delta^{18}O_c$ patterns show that the specimens record 3 (*A. incurva* and *B. suecicus*) to 6 (*R. diluvianum*) full years of growth. Clumped isotope analyses on small aliquots yielded Δ_{47} ranges between 0.62–0.73‰ for *R. diluvianum*, 0.64–0.76‰ for *A. incurva,* and 0.63–0.75‰ for *B. suecicus*. Summaries of measurement results are displayed in Table 1.

Detailed step-by-step results of the data processing routine are shown in ref. [17], in Supplementary Methods and Supplementary Figs. S2–3. Figure 2 and Table 1 show monthly Δ_{47}, SST and $\delta^{18}O_{sw}$ reconstructions for each specimen. Uncertainties at the 95% confidence level on monthly SST vary between 1.8 and 4.2 °C owing to variable monthly sampling density related to intra-shell growth rate variability (Fig. 2). While variations in growth rate (Fig. 2A) caused differences in the sample size between monthly time bins, combining data from the same month in multiple growth years allowed reliable SST and $\delta^{18}O_{sw}$ reconstructions for all monthly time bins in each specimen. Calculations of mean annual temperature (MAT) and seasonality from these monthly averages eliminate seasonal bias due to growth rate variability. Statistically significant ($p < 0.01$) SST seasonality was observed in all specimens. Summer and winter temperatures, defined as mean temperatures of the warmest and coldest month, in *A. incurva* (13 ± 2–26 ± 4 °C) and *B. suecicus* (14 ± 4–25 ± 3 °C) are statistically indistinguishable ($p > 0.2$), while SST from *R. diluvianum* are significantly higher (20 ± 2–29 ± 2 °C; $p < 0.05$). Significant $\delta^{18}O_{sw}$ seasonality was found in *R. diluvianum* (0.0 ± 0.3–1.1 ± 0.3‰VSMOW; $p < 0.01$) and *B. suecicus* (−1.8 ± 0.8–0.6 ± 0.5‰ VSMOW; $p < 0.01$), but not in *A. incurva* (−0.9 ± 0.2 to −0.4 ± 0.9‰VSMOW; $p = 0.07$; Fig. 2; Table 1). *R. diluvianum* records significantly higher $\delta^{18}O_{sw}$ values ($p < 0.01$) than the other specimens. In all specimens, monthly $\delta^{18}O_{sw}$ positively correlates with monthly SST (see Fig. 2).

We compare reconstructed SST from this and previous studies with local and global Campanian SSTs modeled using the HadCM3BL-M2.1aE model[36]. Our model has been improved from being highly utilized in IPCC intercomparison assessment reports and compares well with CMIP5-generation model for many variables, including surface temperature[36]. Importantly for this work, it is sufficiently computationally efficient to allow the long simulations required to reach close to equilibrium for paleoclimates[19] (see "Methods"). We present global Campanian latitudinal gradients in summer, winter, and MAT (Fig. 3A) as well as monthly SST in the Boreal Chalk Sea (Fig. 3B) for both 2× and 4× preindustrial atmospheric pCO_2 simulations (see "Methods"). Model results are summarized in Supplementary Data 5. The modeled Campanian latitudinal SST gradient (difference between tropics and high-latitude MAT; 26 °C in both simulations) resembles the modern (25 °C gradient). Modeled global mean Campanian SST seasonality (difference between warmest and coldest month) is lower (6.6 °C) than that of the modern ocean (8.6 °C) under 2× preindustrial pCO_2 conditions and resembles the present (8.2 °C) in the 4× preindustrial pCO_2 simulation, corroborating recent studies arguing against the hypothesis of reduced seasonality during greenhouse

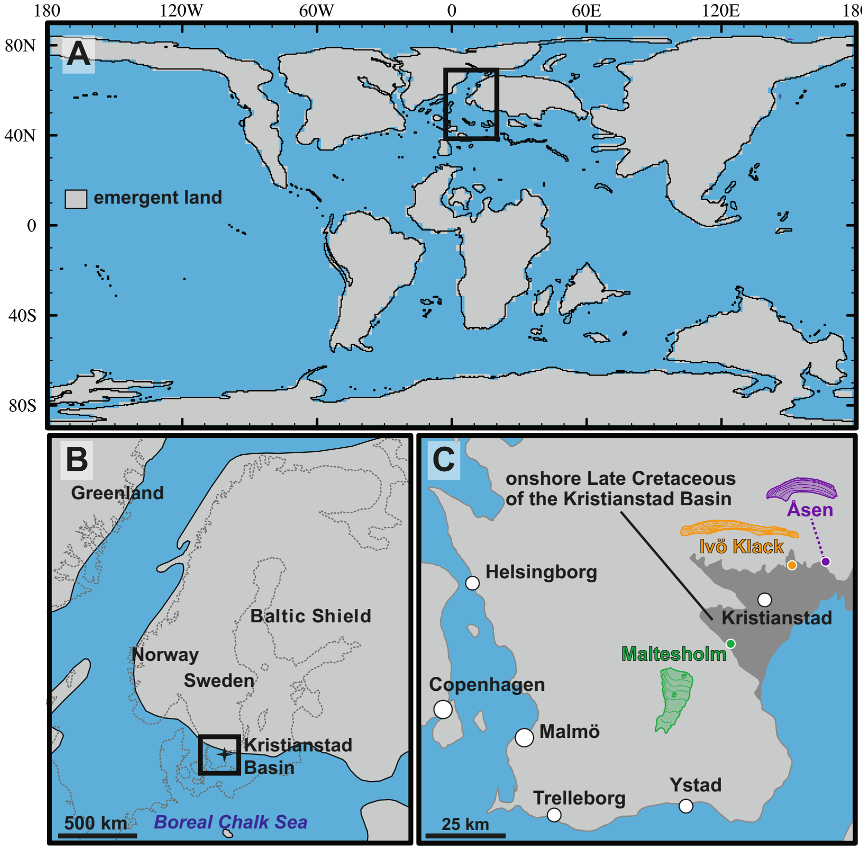

Fig. 1 Campanian (78 million years ago) paleogeography and geological setting. A Global paleogeography used in climate model[19] **B** Northern Europe, black star indicates the Kristianstad Basin **C** Southern Sweden with Kristianstad Basin (in dark gray, submerged in the Campanian). Colored dots indicate the three sampled localities on the paleoshoreline with schematic representations of the species. In all maps, blue color indicates sea surface and light gray indicates emergent land. Maps (**B**) and (**C**) are adapted from ref. [46].

conditions[16,37]. Campanian modeled MAT is ~18 °C and ~22 °C under 2× and 4× preindustrial atmospheric pCO_2, respectively, compared to ~14 °C in the modern ocean[38], yielding an equilibrium climate sensitivity, or global warming per doubling of atmospheric CO_2 concentration, of ~4 °C[19]. Specifically, simulated seasonal SST ranges in the Campanian Kristianstad Basin of 7 ± 3–20 ± 2 °C for 2× and 12 ± 2–26 ± 2 °C for 4× preindustrial atmospheric pCO_2 forcing are significantly warmer than present day (3 ± 0.8–17 ± 0.4 °C[38]) and modeled pre-industrial local SST seasonality (−1.6 to +11.2 °C[19]).

Discussion

Comparison between specimens. Our novel Δ_{47}-based monthly SST and $\delta^{18}O_{sw}$ reconstructions from *A. incurva* and *B. suecicus* are statistically indistinguishable from 4× preindustrial pCO_2 simulations ($p > 0.05$) and significantly warmer than the 2× preindustrial pCO_2 simulations (>4 °C higher MAT, $p < 0.05$) of local SST seasonality (Fig. 3). Higher ($p < 0.05$) SST (+4–5 °C) and $\delta^{18}O_{sw}$ (+1.0–1.5‰) in *R. diluvianum* are likely caused by local differences in its shallower, inter-tidal (<5 m) environment[35]. Temporary areal exposure during low tides could have elevated temperatures and $\delta^{18}O_{sw}$ recorded in *R. diluvianum* year-round by direct sunlight and evaporation, as in modern inter-tidal oyster species[39]. By comparison, the deeper (5–15 m) subtidal environments of *A. incurva* and *B. suecicus* were unaffected by these processes and may have received more water with an open marine $\delta^{18}O_{sw}$ signature (closer to the −1‰VSMOW assumed for ice-free oceans[40]), especially in winter. Such local environmental differences are not resolved in the climate model simulations but show the unprecedented detail of local SST and $\delta^{18}O_{sw}$ reconstructions from clumped isotope analyses in bivalve shells (see Supplementary Discussion). The ~1‰ $\delta^{18}O_{sw}$ seasonality shows that summers in the Campanian Kristianstad Basin either experienced excess evaporation, which increases $\delta^{18}O_{sw}$ by preferentially removing isotopically light seawater, or reduced precipitation, which supplies isotopically light meteoric water, reducing $\delta^{18}O_{sw}$. Both processes lead to comparatively dry summers and wet winters.

Bias due to $\delta^{18}O_{sw}$ assumptions. Strong seasonal fluctuations in $\delta^{18}O_{sw}$ (up to 1.3‰ in *B. suecicus*) and regular deviations from the commonly assumed −1‰VSMOW $\delta^{18}O_{sw}$ value lead to large differences (up to 8.9 °C in *R. diluvianum*) between SST estimates based on Δ_{47} and $\delta^{18}O_c$ (Fig. 2). The risk of assuming constant $\delta^{18}O_{sw}$ is even more clearly illustrated by significantly (+3.5–6.0 °C) higher $\delta^{18}O_c$-based seasonal temperature reconstructions for *B. suecicus* compared to *A. incurva*, while both specimens grew under similar SST seasonality conditions (Fig. 2B). Similarly, $\delta^{18}O_c$-based temperature reconstructions of *A. incurva* and *R. diluvianum* are indistinguishable, while the paleoenvironment of *R. diluvianum* was 4–5 °C warmer year-round (Fig. 2B). This illustrates that the constant $\delta^{18}O_{sw}$ assumption is only valid in settings with negligible $\delta^{18}O_{sw}$ seasonality and where $\delta^{18}O_{sw}$ is known. Low-latitude Tethyan SST seasonality reconstructions based on rudist $\delta^{18}O_c$[15] agree with model simulations, which may indicate that $\delta^{18}O_{sw}$ seasonality is less important in open marine settings. However, data–model agreement is by no means solid evidence for correct $\delta^{18}O_{sw}$ assumptions, which should always be

Table 1 Overview of analytical results ($\delta^{18}O_c$ and Δ_{47}) and reconstructions.

Species (locality)	age [yr]	Measurement results								Monthly reconstructions					
			$\delta^{18}O_c$ [‰VPDB]		Δ_{47}		Δ_{47} [‰]			$\delta^{18}O_{sw}$ [‰VSMOW]			SST [°C]		
		N	min.	mean	max	N	min.	mean	max	CM	MA	WM	CM	MA	WM
R. diluvianum (Ivö Klack)	6.2	198	−1.77 *±0.25*	−1.27 *±0.08*	−0.82 *±0.16*	121	0.658 *±0.007*	0.674 *±0.003*	0.691 *±0.006*	0.00 *±0.27*	0.56 *±0.11*	1.08 *±0.36*	19.6 *±1.8*	24.6 *±0.7*	29.2 *±2.3*
A. incurve (Åsen)	3.3	150	−2.12 *±0.02*	−0.77 *±0.12*	−0.17 *±0.22*	115	0.670 *±0.014*	0.703 *±0.004*	0.716 *±0.008*	−0.89 *±0.18*	−0.46 *±0.09*	−0.36 *±0.87*	12.7 *±2.3*	16.4 *±0.7*	25.7 *±4.2*
B. suecicus (Maltesholm)	3	178	−2.40 *±0.16*	−1.89 *±0.07*	−1.35 *±0.13*	102	0.672 *±0.009*	0.692 *±0.005*	0.713 *±0.015*	−1.81 *±0.78*	−1.18 *±0.17*	−0.55 *±0.45*	13.7 *±3.9*	19.3 *±0.9*	24.8 *±2.6*

All uncertainties are given as 95% confidence levels, species names are provided in italics.
N number of measurements, the age is estimated from the age modeling results (Supplementary Data 2), *CM* coldest month, *MA* mean annual, *WM* warmest month. $\delta^{18}O_c$ carbonate oxygen isotope value, $\delta^{18}O_{sw}$ seawater oxygen isotope value, Δ_{47} clumped isotope value.

independently verified (Fig. 3A). Our findings corroborate previous Δ_{47}-based and proxy comparison studies which also report a significant cold bias (~−8 °C) in $\delta^{18}O_c$-based SST reconstructions due to inaccurate $\delta^{18}O_{sw}$ assumptions and seasonal bias[12,41]. It must be noted that non-carbonate temperature proxies (e.g. based on organic chemistry or palaeobotanical evidence) rely on assumptions other than $\delta^{18}O_{sw}$ which may also bias reconstructions.

Seasonal bias. Seasonal variability in growth rates in all specimens (Fig. 2A) illustrates how bulk sampling of bio-archives can lead to significant biases in MAT reconstructions compared to our more accurate estimates of MAT as an average of Δ_{47}-based monthly SST. In this case, considerable differences in growth rate and $\delta^{18}O_{sw}$ seasonality between specimens would cause an unpredictable bias in MAT between −7.8 °C and +1.4 °C (Fig. 2A; Supplementary Data 3). Indeed, our Campanian mid-latitude SST ranges (~15–27 °C, MAT of 20 °C) are significantly higher than previous SST reconstructions of the same paleolatitude based on fish tooth $\delta^{18}O_c$ (15–20 °C[42]), chalk $\delta^{18}O_c$ (12–15 °C[13]), bulk mollusk Δ_{47} (5–12 °C[25]), TEX_{86} (15–20 °C[12]) and sub-annual mollusk $\delta^{18}O_c$ (15–22 °C;[34] Fig. 3A). On average, these previous studies yield lower MAT (~15 °C) than our seasonally controlled reconstructions and model (see Supplementary Discussion and Supplementary Fig. S4), but they highlight considerable variability between localities, even within the same study[25] (Supplementary Discussion). The proxies used in these studies are affected differently by either seasonal or $\delta^{18}O_{sw}$ bias, or both. An additional source of cold bias affecting carbonate microfossil (most notably chalk) records is mixing of biogenic carbonate with carbonate cements precipitated under cooler sea floor conditions during early diagenesis[41,43].

Given the increase in frequency and duration of growth stops in modern mollusks with increasing latitude[21], seasonal biases are likely more common in higher latitude environments. Since shallow marine bio-archives can record local climate conditions at higher spatial and temporal resolution than conventional (open ocean) archives, our monthly resolved Δ_{47} records present a tool for eliminating widespread biases related to seasonal variability and $\delta^{18}O_{sw}$ assumptions on SST reconstructions across time and space by combining long-term MAT reconstructions with snapshots of climate on the seasonal scale. The average seasonal range reconstructed from our three specimens (15–27 °C range, MAT of 20 °C) likely represents the most accurate SST seasonality reconstructions for the Campanian Boreal Chalk Sea to date. The reconstructions are supported by the remarkable agreement between Δ_{47}-based SST ranges and climate model simulations. Late Cretaceous reconstructions from the same latitude yield similar terrestrial MATs with higher seasonality[37], analogous to modern terrestrial-marine contrast (see Supplementary Discussion), and corroborate our findings of warmer, highly seasonal Late Cretaceous climate.

Data-model comparison. Robust agreement between our reconstructions and the 4× preindustrial pCO_2 model simulation down to the monthly scale provides strong evidence for considerably (up to ~8 °C) warmer higher latitudes during the Late Cretaceous greenhouse compared to the present day. Significant disagreement between summer, winter, and annual SST reconstructions from every specimen in this study and the 2× preindustrial pCO_2 simulation strongly favor higher (4× preindustrial pCO_2) radiative forcing (see Supplementary Data 4). Point-by-point data-model comparisons show that most previous Late Cretaceous SST reconstructions from the same latitudes yield lower temperatures with lesser data-model agreement

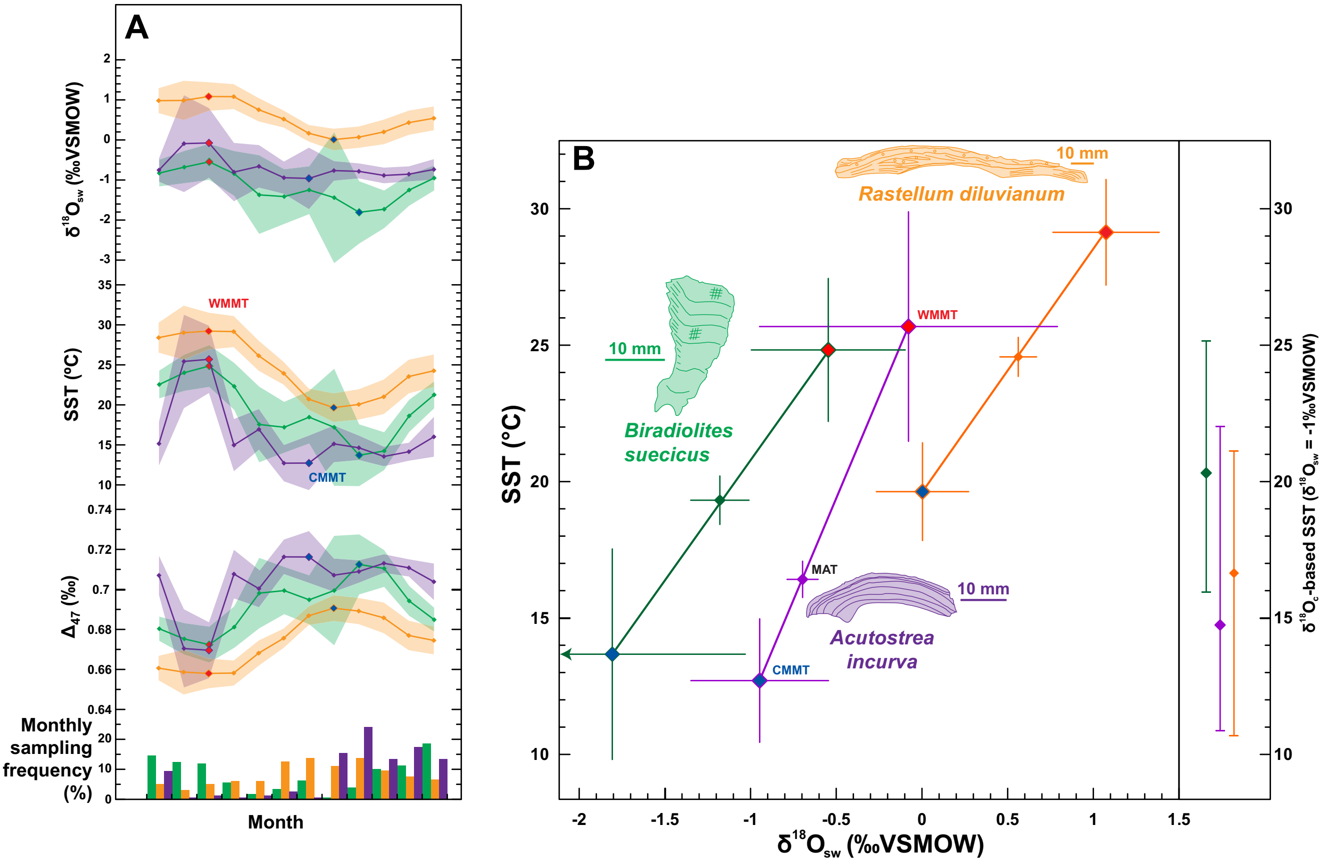

Fig. 2 Paleoseasonality reconstructions. A From bottom to top: relative monthly sampling frequencies reflecting growth rate variability (bar chart), monthly average clumped isotope value (Δ_{47}), sea surface temperature (SST) and seawater oxygen isotope value ($\delta^{18}O_{sw}$) reconstructions from *R. diluvianum* (orange), *A. incurva* (purple) and *B. suecicus* (green). Shaded envelopes indicate 95% confidence levels. Red and blue dots respectively indicate warmest and coldest months. **B** SST and $\delta^{18}O_{sw}$ reconstructions of warmest month (red symbols), coldest month (blue symbols) and annual average (symbols in color of specimen). Thin crosses indicate 95% confidence level uncertainties. Vertical bars on the right indicate summer, winter, and mean annual temperature (MAT) estimates from carbonate oxygen isotope values ($\delta^{18}O_c$; assuming constant $\delta^{18}O_{sw}$ of −1‰VSMOW[40]). Cross-sections through specimens are drawn with horizontal 10 mm scale bars.

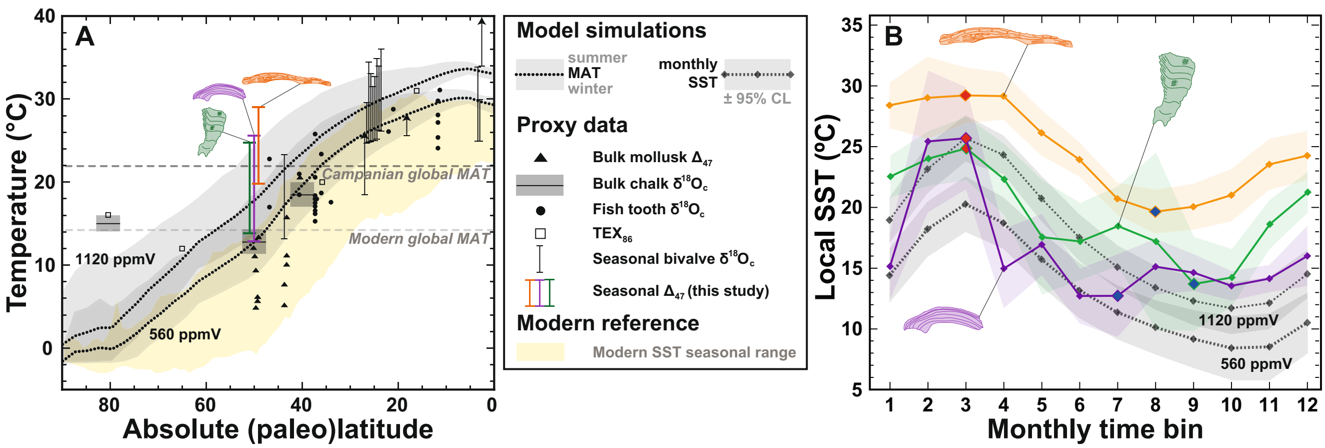

Fig. 3 Comparison between model and reconstructions. A Campanian latitudinal sea surface temperature (SST) gradient with vertical orange, purple and green bars showing seasonality reconstructions from this study and dashed black lines indicating modeled mean annual temperatures (560 ppmV = 2× preindustrial and 1120 ppmV = 4× preindstrial CO_2 pressure) with gray envelopes representing seasonality. Black symbols and bars show previous SST reconstructions[11–13,15,25,42,68,69]. The large range in bulk mollusk clumped isotope (Δ_{47})-based SST estimates is discussed in Supplementary Discussion. The shaded yellow envelope indicates modern seasonal SST range (NOAA, 2021). Horizontal dashed lines mark modern and Campanian global mean annual temperature (MAT). **B** Monthly SST reconstructions (in orange, purple and green) and local model outputs (in gray) in the Boreal Chalk Sea. Diamonds indicate monthly SST means, with red and blue diamonds showing monthly summer and winter extremes, respectively. Shaded envelopes show 95% confidence levels and color coding follows Fig. 2.

(Supplementary Discussion). Bio-archives from mid to high latitudes are likely much more sensitive to $\delta^{18}O_{sw}$ and seasonality bias than low-latitude records[21,25], contributing to the flawed paradigm of shallow latitudinal temperature gradients during greenhouse climates. Our results concur with the recent trend of converging data and model reconstructions yielding modern-scale Late Cretaceous latitudinal temperature gradients[16,42], thereby challenging the hypothesis of "equable climate" during greenhouse periods[14] (see Supplementary Discussion). Moreover, our unique absolute monthly SST reconstructions and model simulations corroborate growing evidence against the hypothesis of reduced temperature seasonality in greenhouse climates[37]. Future work should aim to further test these hypotheses by applying the clumped isotope seasonality method on bio-archives from a range of latitudes in greenhouse climate periods. Results from *B. suecicus* represent the first Δ_{47}-based SST reconstructions from rudist bivalves, introducing an abundant archive and method with which to explore latitudinal seasonality gradients throughout the Mesozoic and across different ocean basins[15].

Conclusions

Our new absolute temperature seasonality reconstructions merit critical evaluation of classical paleoclimate records that risk bias, such as those based on $\delta^{18}O_c$ (assuming constant $\delta^{18}O_{sw}$[11,13]), bulk analyses of fossil material with growth seasonality (e.g. mollusks and brachiopods[25,27]) or a fixed growth season (e.g. planktic foraminifera[44]) and organic proxies that may be seasonally biased (e.g. TEX_{86} and $U^{k'}_{37}$[8,45]). In addition, our monthly $\delta^{18}O_{sw}$ reconstructions for the first time allow evaluation of local seasonality in the hydrological cycle from accretionary bio-archives, revealing dry summers and wet winters in the Campanian Kristianstad Basin. This unique advantage of Δ_{47}-based seasonality reconstructions enables the reconstruction of previously unknown high-resolution variability in salinity, local precipitation, and evaporation in past climates. Combined with longer-term, global-scale paleoclimate records and models, our new method for absolute monthly SST and $\delta^{18}O_{sw}$ reconstructions has the potential to resolve critical disagreements between SST proxies, reduce biases of deep-time paleoclimate reconstructions, shed light on new aspects of past climate seasonality and reconcile proxy reconstructions and model simulations of greenhouse climate.

Methods

Geological setting. The bivalve specimens used in this study were obtained from the Ivö Klack (*R. diluvianum*), Åsen (*A. incurva*) and Maltesholm (*B. suecicus*) localities in the Kristianstad Basin[35,46] in southern Sweden (56°2′ N, 14° 9′ E; 46 ± 3°N paleolatitude based on paleorotation by;[47] see Fig. 1 and Supplementary Data 7). The three distinct localities contain a rich (>200 species), well-preserved Campanian rocky shore fauna[35,46] and were all deposited at the peak of transgression of the latest early Campanian, as supported by the restriction of these deposits to the *Belemnellocamax mammillatus* belemnite biozone and Sr-isotope chemostratigraphy[35,46,48]. The tectonic quiescence of the region since the Late Cretaceous limited burial and promoted excellent shell preservation[34,35]. Burial of loosely compacted sediments of the studied localities was limited to a maximum of 40 m[35]. We can therefore conclude that burial temperatures never exceeded 80 °C and that solid-state reordering did not affect clumped isotope results from these specimens[49,50] (see Supplementary Methods). The Kristianstad Basin represents the highest latitude location for the occurrence of rudist bivalves known to date[46].

Materials. Fossil *R. diluvianum* oysters were found in situ clinging to the sides of large boulders at a paleodepth of <5 m[46], while the *B. suecis* rudist and *A. incurva* oysters were found in life position in a deeper setting (5–15 m) among skeletal fragments on the paleo-seafloor[51] (see Supplementary Methods). The preservation of multiple specimens from this site (including the ones used here) was demonstrated through electron and visible light microscopy, trace element (e.g. Sr/Ca and Mn/Ca) analyses and ultrastructure preservation, results of which are reported in detail in[34] and[51] and summarized in Supplementary Methods and Supplementary Fig. S1.

Sampling. Powdered samples (~300 µg) were drilled in growth direction from polished cross sections through the shell's axis of maximum growth using a Dremel® 3000 rotary drill (Robert Bosch Ltd., Uxbridge, UK) operated at slow rotation equipped with a 300 µm wide tungsten carbide drill bit. High (~100 µm) uniform sampling resolution was achieved by careful abrasive drilling using the side of the drill parallel to the growth lines in the shell. In oyster shells, the well-preserved dense foliated calcite was targeted[52], while in the rudist the dense outer calcite was sampled, avoiding the honeycomb structure in the inner part of the outer shell layer which is more susceptible to diagenetic alteration[53]. A total of 145 samples was obtained from which 338 aliquots of ~100 µg was analyzed (see Table 1).

Clumped isotope analyses. Clumped isotope (Δ_{47}) analyses were carried out on Thermo Fisher Scientific MAT253 and 253 Plus mass spectrometers coupled to a Kiel IV carbonate preparation devices. Calcite samples (individual replicates of ~90 µg for MAT253 Plus and ~150 µg for MAT253) were reacted at 70 °C with nominally anhydrous (103%) phosphoric acid. The resulting CO_2 gas was cleaned from water and organic compounds with two cryogenic LN2 traps and a PoraPak Q trap kept at −40 °C. The purified sample gases were analyzed in micro-volume LIDI mode with 400 s integration time against a clean CO_2 working gas ($\delta^{13}C = -2.82‰$; $\delta^{18}O = -4.67‰$), corrected for the pressure baseline[54–56] and converted into the absolute reference frame by creating an empirical transfer function from the daily analyzed ETH calcite standards (ETH-1, -2, -3) and their accepted values[31]. We measured more ETH-3 standards to better constrain uncertainties around expected Δ_{47} values of our samples[57]. All isotope data were calculated using the new IUPAC parameters following[58] and Δ_{47} values were projected to a 25 °C acid reaction temperature with a correction factor of 0.071 ‰[59]. Long-term Δ_{47} reproducibility standard deviation was 0.04‰ (0.039‰ for MAT253 Plus and 0.045‰ for MAT253; combined uncertainty of 0.077‰ at the 95% confidence level) based on repeated measurements of ~100 µg aliquots of our check standard IAEA C2 (Δ_{47} of 0.719‰; measured over a 20-month period; see Supplementary Data 8 for details). No statistical difference was found between results from both instruments (see Supplementary Data 8). For the $\delta^{18}O_c$ compositions we applied an acid correction factor of 1.00871[22] and reported versus VPDB with a typical reproducibility below 0.13‰ (95% confidence level). Results were combined with $\delta^{18}O_c$ data previously measured in the same shells[34,51] (Supplementary Data 2) to improve the confidence of seasonal age models and the temporal resolution of SST and $\delta^{18}O_{sw}$ reconstructions.

Absolute paleoseasonality reconstructions. We reconstructed absolute SST seasonality by aligning Δ_{47} data relative to the seasonal cycle observed in $\delta^{18}O_c$ using an age modeling routine[60] (Supplementary Data 1 and 9). Note that while chronologies were based on seasonal oscillations in $\delta^{18}O_c$ records, the resulting age model is not compromised by unconstrained seasonal variability in $\delta^{18}O_{sw}$ (see discussion in ref. [17], Supplementary Methods and Supplementary Figs. S2–3). Since only the shape of the seasonal oscillations in $\delta^{18}O_c$ is used for age modeling, age model results are independent from the absolute SST and $\delta^{18}O_{sw}$ seasonality and yield accurate results as long as the shape of the $\delta^{18}O_c$ curve exhibits annual cyclicity[17,60] (Supplementary Methods). We used a statistical approach to combine aliquots for Δ_{47}-based seasonality reconstructions. A step-by-step explanation of our Δ_{47}-$\delta^{18}O_c$ seasonality routine as well as a detailed evaluation of its precision and accuracy on a range of Δ_{47}-$\delta^{18}O_c$ datasets is provided in[17] and in Supplementary Methods. R functions used to calculate seasonality from the sample size optimization routine are compiled into the documented R package *seasonalclumped* and deposited in the open-source R code repository CRAN[61]. The number of 100 µg Δ_{47} aliquots to combine into monthly SST estimates is optimized by grouping aliquots from the same month in different growth years. Analytical uncertainties are propagated through this optimization procedure using Monte Carlo simulations (details in Supplementary Methods and Supplementary Data 10). SSTs are calculated from Δ_{47} values in monthly time bins (1/12th of the seasonal cycle) using the temperature calibration by[62] recalculated in ref. [31], and $\delta^{18}O_{sw}$ is reconstructed from Δ_{47}-SST and $\delta^{18}O_c$ following[22] (Supplementary Methods and Supplementary Data 3). Tests on a diverse group of modern datasets in ref. [17] demonstrate that this method achieves the ideal compromise between eliminating bias and retaining high reproducibility while keeping SST and $\delta^{18}O_{sw}$ reconstructions independent of the $\delta^{18}O_c$ values on which the age model is based (see also Supplementary Methods). The clumped isotope temperature calibration by ref. [31] is statistically indistinguishable from the temperature relationship based on theoretical principles within the temperature range discussed in ref. [32] and is the culmination of recent convergence of measurement results between labs across the world and inter-lab standardization efforts[32,59,63]. Seasonality is defined as the difference between the average temperatures in the warmest and coldest month, while mean annual temperature (MAT) is expressed as the average of all monthly temperatures, following USGS definitions[64]. Statistical analyses of seasonality, differences between specimens and differences between data and model are summarized in Supplementary Data 4.

Climate model. We utilize a fully equilibrated (>11,000 model years) paleoclimate model (HadCM3BL-M2.1aE) Campanian (78 Ma) simulation. Model boundary conditions (topography, bathymetry, solar luminosity) for the Campanian are the same as in[19]. We evaluate model simulations with radiative forcing (pCO_2) set to 560 ppmV (2× preindustrial concentration) and 1120 ppmV (4× preindustrial concentration), within the range of pCO_2 reconstructions for the Campanian as compiled by ref. [65], and a modern astronomical configuration with dynamic vegetation. HadCM3 is, to our knowledge, the only model to run Campanian-specific boundary conditions with a range of pCO_2 forcing out to full equilibrium. This is critical as it was shown that the deep ocean and hence ocean circulation can take at least 5000 modeled years to fully equilibrate to the applied boundary conditions[19], casting doubt on the validity of alternative model simulations that did not attain equilibrium. The model also compares well with CMIP5-generation model for many variables, including surface temperature[36]. Details on the HadCM3L model are provided in Supplementary Methods and in ref. [19]. Local seasonal SSTs are calculated for the paleorotated Kristianstad Basin[47] (42.5-50°N, 7.5-15°E; Supplementary Data 5) from averages of the upper ocean grid boxes in the model simulation. The model has a spatial resolution of 3.75° × 2.5° and uses 20 layers in ocean depth, of which the upper ocean box averages the top 10 m of the ocean. Hence the average SST of the Kristianstad Basin is biased against the shallowest coastal regions of the basin, such as the locality of *R. diluvianum*[66,67]. For comparison, modern SST data come from the National Oceanic and Atmospheric Administration[38] (Supplementary Data 6 and Supplementary Methods).

Data availability

Extended methods, data and scripts belonging to this study are available in the open-access database Zenodo (https://doi.org/10.5281/zenodo.3865428). This online database contains the following Supplementary Data files:

Supplementary Data 1: Raw results of growth modelling
Supplementary Data 2: Raw clumped isotope results
Supplementary Data 3: Results of statistical sample grouping protocol
Supplementary Data 4: Overview statistical test results
Supplementary Data 5: Modelled sea surface temperature data
Supplementary Data 6: Modern sea surface temperature data
Supplementary Data 7: Paleolatitude evolution of the Kristianstad Basin
Supplementary Data 8: Results of reproducibility tests for clumped isotope analyses
Supplementary Data 9: Matlab age modelling script
Supplementary Data 10: R script for statistical sample grouping

Code availability

Matlab scripts used to produce shell age models are provided in Supplementary Data 9. R scripts used to calculate monthly SST and $\delta^{18}O_{sw}$ values from Δ_{47} and $\delta^{18}O_c$ data provided in Supplementary Data 10 and are compiled in the documented *seasonalclumped* package uploaded to the open-course R package repository CRAN[61].

Received: 14 December 2020; Accepted: 19 May 2021;
Published online: 10 June 2021

References

1. Marshall, D. J. & Burgess, S. C. Deconstructing environmental predictability: seasonality, environmental colour and the biogeography of marine life histories. *Ecol. Lett.* **18**, 174–181 (2015).
2. Matthews, T., Mullan, D., Wilby, R. L., Broderick, C. & Murphy, C. Past and future climate change in the context of memorable seasonal extremes. *Clim. Risk Manag.* **11**, 37–52 (2016).
3. Carré, M. & Cheddadi, R. Seasonality in long-term climate change. Quaternaire. Revue de l'Association française pour l'étude du Quaternaire 173–177 https://doi.org/10.4000/quaternaire.8018 (2017).
4. Lovejoy, T. E. *Climate Change And Biodiversity*. (TERI Press, New Delhi, India, 2006).
5. Parmesan, C. Ecological and evolutionary responses to recent climate change. *Annu. Rev. Ecol. Evol. Syst.* **37**, 637–669 (2006).
6. Harsch, M. A. & Hille Ris Lambers, J. Climate warming and seasonal precipitation change interact to limit species distribution shifts across Western North America. *PLoS ONE* **11**, e0159184 (2016).
7. Zeebe, R. E., Zachos, J. C. & Dickens, G. R. Carbon dioxide forcing alone insufficient to explain Palaeocene–Eocene Thermal Maximum warming. *Nat. Geosci.* **2**, 576 (2009).
8. Cramwinckel, M. J. et al. Synchronous tropical and polar temperature evolution in the Eocene. *Nature* **559**, 382 (2018).
9. IPCC. IPCC, 2013: Climate Change 2013: The Physical Science Basis. Contribution of Working Group I to the Fifth Assessment Report of the Intergovernmental Panel on Climate Change, 1535 pp. (Cambridge Univ. Press, Cambridge, UK, and New York, 2013).
10. Tierney, J. E. et al. Past climates inform our future. *Science* **370**, eaay3701 (2020).
11. Jenkyns, H. C., Forster, A., Schouten, S. & Damsté, J. S. S. High temperatures in the late Cretaceous Arctic Ocean. *Nature* **432**, 888 (2004).
12. O'Brien, C. L. et al. Cretaceous sea-surface temperature evolution: constraints from TEX86 and planktonic foraminiferal oxygen isotopes. *Earth-Sci. Rev.* **172**, 224–247 (2017).
13. Thibault, N., Harlou, R., Schovsbo, N. H., Stemmerik, L. & Surlyk, F. Late Cretaceous (late Campanian–Maastrichtian) sea-surface temperature record of the Boreal Chalk Sea. *Clim. Past* **12**, 429–438 (2016).
14. Huber, B. T., Hodell, D. A. & Hamilton, C. P. Middle–Late Cretaceous climate of the southern high latitudes: stable isotopic evidence for minimal equator-to-pole thermal gradients. *Geol. Soc. Am. Bull.* **107**, 1164–1191 (1995).
15. Steuber, T., Rauch, M., Masse, J.-P., Graaf, J. & Malkoč, M. Low-latitude seasonality of Cretaceous temperatures in warm and cold episodes. *Nature* **437**, 1341–1344 (2005).
16. Upchurch, G. R. Jr, Kiehl, J., Shields, C., Scherer, J. & Scotese, C. Latitudinal temperature gradients and high-latitude temperatures during the latest Cretaceous: Congruence of geologic data and climate models. *Geology* **43**, 683–686 (2015).
17. de Winter, N., Agterhuis, T. & Ziegler, M. Optimizing sampling strategies in high-resolution paleoclimate records. *Clim. Past Discuss.* https://doi.org/10.5194/cp-2020-118 (2020).
18. Joussaume, S. & Braconnot, P. Sensitivity of paleoclimate simulation results to season definitions. *J. Geophys. Res.: Atmos.* **102**, 1943–1956 (1997).
19. Farnsworth, A. et al. Climate sensitivity on geological timescales controlled by nonlinear feedbacks and ocean circulation. *Geophys. Res. Lett.* **46**, 9880–9889 (2019).
20. Mosbrugger, V. Nearest-living-relative method. Encyclopedia of paleoclimatology and ancient environments 607–609 (2009).
21. Lartaud, F. et al. A latitudinal gradient of seasonal temperature variation recorded in oyster shells from the coastal waters of France and The Netherlands. *Facies* **56**, 13 (2009).
22. Kim, S.-T. & O'Neil, J. R. Equilibrium and nonequilibrium oxygen isotope effects in synthetic carbonates. *Geochim. Cosmochimica Acta* **61**, 3461–3475 (1997).
23. Poulsen, C. J., Barron, E. J., Peterson, W. H. & Wilson, P. A. A reinterpretation of Mid-Cretaceous shallow marine temperatures through model-data comparison. *Paleoceanography* **14**, 679–697 (1999).
24. LeGrande, A. N. & Schmidt, G. A. Global gridded data set of the oxygen isotopic composition in seawater. *Geophys. Res. Lett.* **33**, L12604 (2006).
25. Petersen, S. V. et al. Temperature and salinity of the Late Cretaceous western interior seaway. *Geology* **44**, 903–906 (2016).
26. Jaffrés, J. B. D., Shields, G. A. & Wallmann, K. The oxygen isotope evolution of seawater: a critical review of a long-standing controversy and an improved geological water cycle model for the past 3.4 billion years. *Earth-Sci. Rev.* **83**, 83–122 (2007).
27. Veizer, J. & Prokoph, A. Temperatures and oxygen isotopic composition of Phanerozoic oceans. *Earth-Sci. Rev.* **146**, 92–104 (2015).
28. Briard, J. et al. Seawater paleotemperature and paleosalinity evolution in neritic environments of the Mediterranean margin: insights from isotope analysis of bivalve shells. *Palaeogeogr. Palaeoclimatol. Palaeoecol.* **543**, 109582 (2020).
29. Caldarescu, D. E. et al. Clumped isotope thermometry in bivalve shells: a tool for reconstructing seasonal upwelling. *Geochim. Cosmochim. Acta* **294**, 174–191 (2021).
30. Eiler, J. M. "Clumped-isotope" geochemistry—The study of naturally-occurring, multiply-substituted isotopologues. *Earth Planetary Sci. Lett.* **262**, 309–327 (2007).
31. Bernasconi, S. M. et al. Reducing uncertainties in carbonate clumped isotope analysis through consistent carbonate-based standardization. *Geochem., Geophys., Geosyst.* **19**, 2895–2914 (2018).
32. Jautzy, J. J., Savard, M. M., Dhillon, R. S., Bernasconi, S. M. & Smirnoff, A. Clumped isotope temperature calibration for calcite: bridging theory and experimentation. *Geochem. Perspectives Lett.* **14**, 36–41 (2020).
33. Fernandez, A. et al. A reassessment of the precision of carbonate clumped isotope measurements: implications for calibrations and paleoclimate reconstructions. *Geochem., Geophys., Geosyst.* **18**, 4375–4386 (2017).
34. de Winter, N. J. et al. Shell chemistry of the boreal Campanian bivalve Rastellum diluvianum; (Linnaeus, 1767) reveals temperature seasonality, growth rates and life cycle of an extinct Cretaceous oyster. *Biogeosciences* **17**, 2897–2922 (2020).
35. Surlyk, F. & Sørensen, A. M. An early Campanian rocky shore at Ivö Klack, southern Sweden. *Cretaceous Res.* **31**, 567–576 (2010).
36. Valdes, P. J. et al. The BRIDGE HadCM3 family of climate models: HadCM3@ Bristol v1. 0. *Geoscientific Model Dev.* **10**, 3715–3743 (2017).
37. Burgener, L., Hyland, E., Huntington, K. W., Kelson, J. R. & Sewall, J. O. Revisiting the equable climate problem during the Late Cretaceous greenhouse using paleosol carbonate clumped isotope temperatures from the Campanian

of the Western Interior Basin, USA. *Palaeogeogr. Palaeoclimatol. Palaeoecol.* **516**, 244–267 (2019).
38. NOAA Physical Sciences Laboratory. https://psl.noaa.gov/.
39. Huyghe, D. et al. New insights into oyster high-resolution hinge growth patterns. *Mar. Biol.* **166**, 48 (2019).
40. Shackleton, N. J. Paleogene stable isotope events. *Palaeogeogr. Palaeoclimatol. Palaeoecol.* **57**, 91–102 (1986).
41. Tagliavento, M., John, C. M. & Stemmerik, L. Tropical temperature in the Maastrichtian Danish Basin: Data from coccolith Δ47 and δ18O. *Geology* **47**, 1074–1078 (2019).
42. Pucéat, E. et al. Fish tooth δ18O revising Late Cretaceous meridional upper ocean water temperature gradients. *Geology* **35**, 107 (2007).
43. Drury, A. J. & John, C. M. Exploring the potential of clumped isotope thermometry on coccolith-rich sediments as a sea surface temperature proxy. *Geochem. Geophys. Geosyst.* **17**, 4092–4104 (2016).
44. Pearson, P. N. et al. Warm tropical sea surface temperatures in the Late Cretaceous and Eocene epochs. *Nature* **413**, 481–487 (2001).
45. Jia, G., Wang, X., Guo, W. & Dong, L. Seasonal distribution of archaeal lipids in surface water and its constraint on their sources and the TEX86 temperature proxy in sediments of the South China Sea. *J. Geophys. Res.: Biogeosci.* **122**, 592–606 (2017).
46. Sørensen, A. M., Surlyk, F. & Jagt, J. W. M. Adaptive morphologies and guild structure in a high-diversity bivalve fauna from an early Campanian rocky shore, Ivö Klack (Sweden). *Cretaceous Res.* **33**, 21–41 (2012).
47. van Hinsbergen, D. J. et al. A paleolatitude calculator for paleoclimate studies. *PLoS ONE* **10**, e0126946 (2015).
48. Christensen, W. K. Paleobiogeography and migration in the Late Cretaceous belemnite family Belemnitellidae. *Acta Palaeontologica Polonica* **42**, 457–495 (1997).
49. Henkes, G. A. et al. Temperature limits for preservation of primary calcite clumped isotope paleotemperatures. *Geochim. Cosmochim. Acta* **139**, 362–382 (2014).
50. Fernandez, A. et al. Reconstructing the magnitude of Early Toarcian (Jurassic) warming using the reordered clumped isotope compositions of belemnites. *Geochim. Cosmochim. Acta* **18**, 4375–4386 (2020). 12.
51. Sørensen, A. M., Ullmann, C. V., Thibault, N. & Korte, C. Geochemical signatures of the early Campanian belemnite Belemnellocamax mammillatus from the Kristianstad Basin in Scania, Sweden. *Palaeogeogr. Palaeoclimatol. Palaeoecol.* **433**, 191–200 (2015).
52. de Winter, N. J. et al. An assessment of latest Cretaceous Pycnodonte vesicularis (Lamarck, 1806) shells as records for palaeoseasonality: a multi-proxy investigation. *Clim. Past* **14**, 725–749 (2018).
53. Pons, J. M. & Vicens, E. The structure of the outer shell layer in radiolitid rudists, a morphoconstructional approach. *Lethaia* **41**, 219–234 (2008).
54. Bernasconi, S. M. et al. Background effects on Faraday collectors in gas-source mass spectrometry and implications for clumped isotope measurements. *Rapid Commun. Mass Spectrom.* **27**, 603–612 (2013).
55. Meckler, A. N., Ziegler, M., Millán, M. I., Breitenbach, S. F. & Bernasconi, S. M. Long-term performance of the Kiel carbonate device with a new correction scheme for clumped isotope measurements. *Rapid Commun. Mass Spectrom.* **28**, 1705–1715 (2014).
56. Müller, I. A. et al. Carbonate clumped isotope analyses with the long-integration dual-inlet (LIDI) workflow: scratching at the lower sample weight boundaries. *Rapid Commun. Mass Spectrom.* **31**, 1057–1066 (2017).
57. Kocken, I. J., Müller, I. A. & Ziegler, M. Optimizing the use of carbonate standards to minimize uncertainties in clumped isotope data. *Geochem. Geophys. Geosyst.* **20**, 5565–5577 (2019).
58. Daëron, M., Blamart, D., Peral, M. & Affek, H. P. Absolute isotopic abundance ratios and the accuracy of Δ47 measurements. *Chem. Geol.* **442**, 83–96 (2016).
59. Petersen, S. V. et al. Effects of improved 17O correction on interlaboratory agreement in clumped isotope calibrations, estimates of mineral-specific offsets, and temperature dependence of acid digestion fractionation. *Geochem. Geophys. Geosyst.* **20**, 3495–3519 (2019).
60. Judd, E. J., Wilkinson, B. H. & Ivany, L. C. The life and time of clams: derivation of intra-annual growth rates from high-resolution oxygen isotope profiles. *Palaeogeogr. Palaeoclimatol. Palaeoecol.* **490**, 70–83 (2018).
61. de Winter, N. J. seasonalclumped: Toolbox for Clumped Isotope Seasonality Reconstructions. https://CRAN.R-project.org/package=seasonalclumped (2021).
62. Kele, S. et al. Temperature dependence of oxygen-and clumped isotope fractionation in carbonates: a study of travertines and tufas in the 6–95 °C temperature range. *Geochim. Cosmochim. Acta* **168**, 172–192 (2015).
63. Anderson, N. T. et al. A unified clumped isotope thermometer calibration (0.5–1,100 °C) using carbonate-based standardization. *Geophys. Res. Lett.* **48**, e2020GL092069 (2021).
64. O'Donnell, M. S. & Ignizio, D. A. Bioclimatic predictors for supporting ecological applications in the conterminous United States. US Geological Survey Data Series 691, (2012).
65. Foster, G. L., Royer, D. L. & Lunt, D. J. Future climate forcing potentially without precedent in the last 420 million years. *Nat. Commun.* **8**, 14845 (2017).
66. Johns, T. C. et al. The second Hadley Centre coupled ocean-atmosphere GCM: model description, spinup and validation. *Clim. Dyn.* **13**, 103–134 (1997).
67. Lunt, D. J. et al. Palaeogeographic controls on climate and proxy interpretation. *Clim. Past* **12**, 1181–1198 (2016).
68. de Winter, N. J. et al. Tropical seasonality in the late Campanian (late Cretaceous): comparison between multiproxy records from three bivalve taxa from Oman. *Palaeogeogr. Palaeoclimatol. Palaeoecol.* **485**, 740–760 (2017).
69. Walliser, E. O., Mertz-Kraus, R. & Schöne, B. R. The giant inoceramid Platyceramus platinus as a high-resolution paleoclimate archive for the Late Cretaceous of the Western Interior Seaway. *Cretaceous Res.* **86**, 73–90 (2018).

Acknowledgements

The authors thank Mattia Tagliavento, Laiming Zhang, and an anonymous reviewer for their comments that have helped improve the manuscript, as well as Heike Langenberg for moderating the review process. We thank Prof. Ethan Grossmann for his helpful comments on a previous version of the manuscript. The authors thank Anne Sørensen and Finn Surlyk for their help with sample acquisition and the Department of Geoscience of the University of Copenhagen for permission for destructive sampling of the specimens for isotope analyses. N.J.W. is funded by the Flemish Research Council (FWO; junior postdoc grant; 12ZB220N) and the European Commission (MSCA Individual Fellowship; UNBIAS project 843011). N.T. acknowledges Carslbergfondet CF16-0457. P.C. would like to acknowledge funding from the VUB Strategic Research grant (internal). The authors would like to thank Bart Lippens for help with sample preparation, Arnold van Dijk for analytical support, and Anne Sørensen for helping with sample collection.

Author contributions

The initial design of the study was conceived by N.J.W., N.T., C.V.U., and M.Z. N.J.W., I.A.M., I.J.K., and M.Z. together were responsible for clumped isotope data acquisition. N.T. and C.V.U. provided samples used in this study. D.J.L. and A.F. ran the climate model and provided in-depth input on model-data integration. N.J.W. and P.C. were responsible for acquiring the funding needed for this study. N.J.W. wrote the first draft of the manuscript and revision. All authors then contributed to the writing process.

Competing interests

The authors declare no competing interests.

Additional information

Supplementary information The online version contains supplementary material available at https://doi.org/10.1038/s43247-021-00193-9.

Correspondence and requests for materials should be addressed to N.J.d.W.

Peer review information *Communications Earth & Environment* thanks the anonymous reviewers for their contribution to the peer review of this work. Primary handling editor: Heike Langenberg. Peer reviewer reports are available.